Flux-Dependent Crossover between Quantum and Classical Behavior in a dc SQUID

S. Butz,[1] A. K. Feofanov,[1,†] K. G. Fedorov,[1,2,‡] H. Rotzinger,[1] A. U. Thomann,[3] B. Mackrodt,[4] R. Dolata,[4] V. B. Geshkenbein,[3] G. Blatter,[3] and A. V. Ustinov[1,2,5,*]

[1]*Physikalisches Institut, Karlsruhe Institute of Technology, 76131 Karlsruhe, Germany*
[2]*National University of Science and Technology MISIS, Moscow 119049, Russia*
[3]*Theoretische Physik, ETH Zurich, 8093 Zürich, Switzerland*
[4]*Physikalisch Technische Bundesanstalt, 38116 Braunschweig, Germany*
[5]*Russian Quantum Center, 100 Novaya, Skolkovo, Moscow Region 143025, Russia*

(Received 14 April 2014; revised manuscript received 19 September 2014; published 11 December 2014)

In a coupled system of one classical and one quantum mechanical degree of freedom, the quantum degree of freedom can facilitate the escape of the whole system. Such unusual escape characteristics have been theoretically predicted as the "Münchhausen effect." We implement such a system by shunting one of the two junctions of a dc SQUID with an additional capacitance. In our experiments, we detect a crossover between quantum and classical escape processes related to the direction of escape. We find that, under varying external magnetic flux, macroscopic quantum tunneling periodically alternates with thermally activated escape, a hallmark of the "Münchhausen effect."

DOI: 10.1103/PhysRevLett.113.247005 PACS numbers: 74.50.+r, 03.65.-w, 05.20.-y, 85.25.Dq

A classical object cannot leave a metastable potential well at zero temperature. In contrast, a quantum object can tunnel out of such a well even at zero temperature. But what happens if a quantum degree of freedom is coupled to a classical degree of freedom? This problem was investigated theoretically in Ref. [1] assuming a weak coupling between the two degrees of freedom. The authors found that the tunneling of the quantum mechanical degree of freedom changes the potential for the classical variable, making it possible for the latter to leave its metastable well. As this effect reminds us of the story about Baron Münchhausen, who claimed to have pulled himself and his horse out of a swamp, the theoretically predicted behavior has been termed "Münchhausen effect."

The experiments presented in this Letter aim at testing the above theoretical idea. We follow the original proposal of using the phase difference across a Josephson junction (JJ) as either a quantum mechanical or classical degree of freedom, depending on its effective "mass" that is proportional to the capacitance of the junction [2,3]. In our experiment, two JJs with largely different capacitances are coupled by a supercurrent flowing in a superconducting loop that forms a dc SQUID.

The time evolution of the phase difference φ across a Josephson junction is analogue to that of a massive particle moving in a washboard potential that is tilted when a bias current is applied. The amplitude of the untilted washboard potential is proportional to the Josephson energy $E_J = \Phi_0 I_c/(2\pi)$, where I_c is the critical current of the JJ and $\Phi_0 = 2.07 \times 10^{-15}$ Wb the magnetic flux quantum. According to the Josephson relations [4], the voltage across the JJ is proportional to the velocity $\dot{\varphi}$ of the particle. As long as it is trapped in one of the metastable potential wells, the average voltage is zero. Once the particle escapes its well and runs down the potential, a voltage drop is induced across the junction. This happens at the switching current $I_{sw} < I_c$, when the bias current through the junction, i.e., the tilt of the potential, is strong enough to lower the barrier sufficiently. The escape characteristics of JJs have been extensively studied in the past and, both the predicted thermal activation (TA) and macroscopic quantum tunneling (MQT) processes, have been observed [5–7].

Here, we investigate the escape properties of a dc SQUID consisting of two JJs with deliberately made nonequal capacitances. A sketch of the circuit is shown in Fig. 1(a). It consists of two nominally identical JJs with critical currents I_c placed in a superconducting loop of inductance L. While the dynamics of junction JJ_2 is determined by its small intrinsic capacitance C, junction JJ_1 is additionally shunted with a large on-chip capacitor $C_0 \gg C$. The virtual particle introduced above moves in a two-dimensional (2D) potential. The capacitive asymmetry translates into an effectively increased mass of the particle, when it moves in the direction corresponding to the phase difference across junction JJ_1.

The effect of asymmetry in a dc SQUID has been of interest for some time. For example, asymmetric damping in a dc SQUID can be used to improve its noise properties [8]. Furthermore, SQUIDs with asymmetric critical currents make it possible to suppress phase diffusion [9] and are employed for measuring JJ circuits with large quantum fluctuations [10,11]. They are also used extensively as readout devices of qubits [12] or even directly as qubits [13].

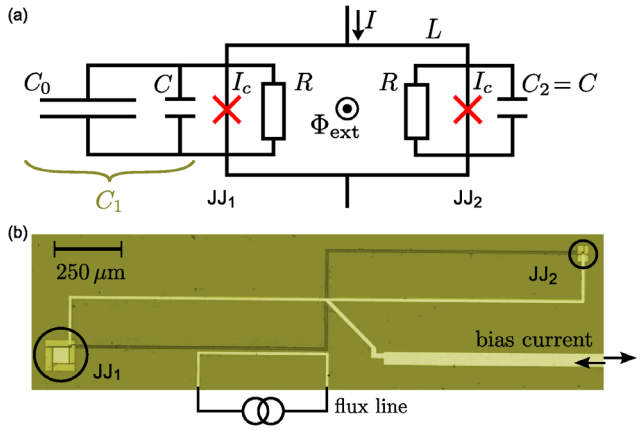

FIG. 1 (color online). (a) Equivalent circuit of the investigated asymmetric dc SQUID. The parameters of the Josephson junctions are their critical currents I_c, normal resistances R, and intrinsic capacitances C. JJ_1 is additionally shunted by a large capacitance C_0. L is the loop inductance of the SQUID. (b) Optical microscope picture of the studied dc SQUID. The bias current lines are fabricated as microstrips one on top of another in order to minimize their mutual inductances with the gradiometric SQUID loop made as a figure of "8".

The equations of motion for the two phase differences φ_1 and φ_2 across the junctions are derived using the resistively and capacitively shunted junction (RCSJ) model:

$$\frac{1}{\omega_{p1}^2}\ddot{\varphi}_1 + \frac{1}{\omega_c}\dot{\varphi}_1 = -\sin\varphi_1 + j - k(\varphi_1 - \varphi_2 - \varphi_{\text{ext}}), \quad (1)$$

$$\frac{1}{\omega_{p2}^2}\ddot{\varphi}_2 + \frac{1}{\omega_c}\dot{\varphi}_2 = -\sin\varphi_2 + j + k(\varphi_1 - \varphi_2 - \varphi_{\text{ext}}). \quad (2)$$

Here, φ_i is the phase difference across the respective junction JJ_i and $\omega_{pi} = \sqrt{2eI_c/(\hbar C_i)}$ is the corresponding plasma frequency. The damping is defined by $1/\omega_c = \hbar/(2eI_cR)$ and $j = I/(2I_c)$ is the normalized bias current through the dc SQUID. The coupling of the two junctions is $k = 1/\beta_L = \Phi_0/(2\pi LI_c)$, and $\varphi_{\text{ext}} = 2\pi\Phi_{\text{ext}}/\Phi_0$ is the phase associated with an externally applied flux Φ_{ext}. Integrating the right-hand side of Eqs. (1) and (2) with respect to both phase differences yields the equation for the normalized 2D potential:

$$v(\varphi_1, \varphi_2) = 2 - \cos\varphi_1 - \cos\varphi_2 - j(\varphi_1 + \varphi_2) + \frac{k}{2}(\varphi_1 - \varphi_2 - \varphi_{\text{ext}})^2. \quad (3)$$

The potential and classical (TA) and quantum mechanical (MQT) escape trajectories are illustrated in Fig. 2. Because of the weak coupling, there are several minima. A classical particle that escapes out of one of those minima follows a trajectory that leads over the lowest barrier [14]. Tunneling, on the other hand, is only possible for $\varphi_1 = \text{const}$ due to the capacitive asymmetry [15].

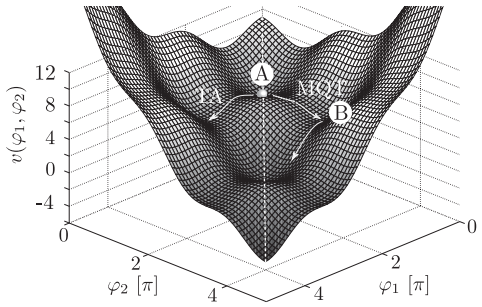

FIG. 2. 2D potential landscape of a dc SQUID with two identical junctions for $k = 0.17$ at a normalized bias current $j = 0.2$ and at $\Phi_{\text{ext}} = 0$. The dashed white line indicates the bisectrix where $\varphi_1 = \varphi_2$.

An optical microscope picture of the dc SQUID is shown in Fig. 1(b). The circuit was fabricated using a submicron $Nb/AlO_x/Nb$ trilayer process [16]. A gradiometric design was used in order to suppress unwanted background noise. The SQUID has a loop inductance $L = 4$ nH, which is distributed symmetrically between the two arms. The two junctions are located at the corners and marked by circles in Fig. 1(b). Their parameters are given in Table I. The critical current $I_{c,\text{nom}}$ stands for the nominally designed critical current and I_{ci} represents the actual critical current extracted from measurement. Details on how the actual (nonidentical) critical currents were determined are given later. The capacitances, plasma frequencies, and the cross-over temperatures are calculated from the measured parameters. The crossover temperature $T_{\text{cr}} = \hbar\omega_p/(2\pi k_B)$ [17] is the temperature at which quantum and thermal escape rates are approximately equal at zero bias current.

The sample was mounted in a dilution cryostat with a base temperature of $T \approx 25$ mK. Extensive filtering of the biasing lines was used in order to reduce high frequency noise. Current ramp measurements [18] were performed for increasing cryostat temperatures starting from 30 mK to obtain the flux-dependent switching characteristics of the asymmetric dc SQUID. The magnetic flux Φ_{ext} was applied by sending current through the on-chip flux line as shown in Fig. 1(b).

For each measured temperature, the flux dependence of the mean switching current I_{sw} is displayed in Fig. 3. The fluctuation free critical current calculated from the measured SQUID parameters is shown by a dashed line.

TABLE I. Parameters of the two junctions of the dc SQUID. $I_{c,\text{nom}}$ refers to the nominal value of the junction, while I_c is the fluctuation-free critical current extracted from measurements. The capacitances of the junctions as well as their respective plasma frequencies and the cross-over temperatures at zero bias are given by C, $\omega_p/(2\pi)$ and T_{cr}, respectively.

	$I_{c,\text{nom}}$ [nA]	I_c [nA]	R [kΩ]	C [fF]	$\omega_p/(2\pi)$ [GHz]	T_{cr} [mK]
JJ_1 (TA)	560	460	3.6	1000	6	46
JJ_2 (MQT)	560	510	3.6	3	115	880

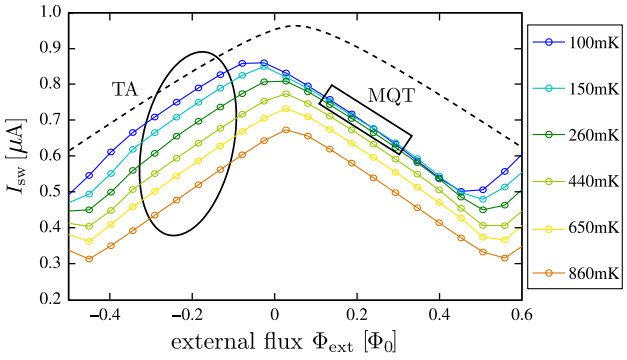

FIG. 3 (color online). Temperature and flux dependence of the mean switching current. Circles indicate measured values, lines are guides to the eye. The black oval and rectangle indicate data points used for the fitting of TA and MQT rates, respectively. The dashed line is the calculated fluctuation free critical current corresponding to the state with zero magnetic flux quanta in the loop. The given temperatures are fit results and deviate from the cryostat temperature as explained later in the text.

Its maximum is shifted from $\Phi_{ext} = 0$ because of the asymmetry in the measured critical currents (cf. Table I). On the left-hand side (positive slope) the lowest temperature curve is close to the zero temperature prediction (dashed line) and a steady decrease of the mean switching current with increasing temperature is observed, consistent with TA predictions. In contrast, on the negative slope the mean switching current is considerably suppressed compared to the dashed line and independent of temperature for the three lowest temperatures. This is a clear indication that the escape on the negative slopes is induced by quantum rather than thermal fluctuations.

This asymmetric dependence of switching current on flux is explained by the direction dependent escape characteristics shown in Fig. 2. At zero bias current and zero flux, the virtual particle describing the state of the system is trapped in the main minimum (location A) which is symmetric with respect to the bisectrix (white dashed line). At temperatures close to zero, the escape along the classical φ_1 direction is allowed only under the condition that the barrier is low, i.e., $j \approx 1$. However, tunneling in the φ_2 direction is possible while the barrier height in that direction is still appreciable. Therefore, as the bias current is increased from zero, the particle leaves well A in the quantum mechanical φ_2 direction and reaches side well B. Further motion in the φ_2 direction from B is inhibited due to the coupling of the two degrees of freedom responsible for the underlying parabolic shape of the potential (cf. Fig. 2). However, the barrier in the φ_1 direction of side well B is much lower than that of A, enabling the escape of the heavy, i.e., classical degree of freedom and thereby the decay of the full system. Thus, the interaction of the two degrees of freedom leads to a suppressed switching current since the tunneling of the quantum degree of freedom facilitates the escape of the classical one.

When increasing the external flux from $\Phi_{ext} = 0$, a circulating current is induced in the SQUID loop. It is oriented such that the net current through JJ_1 is decreased and through JJ_2 increased. Thus, the barrier along φ_2 is decreased and escape due to MQT is possible already at smaller bias currents. However, at the same time the barrier of the side well B in the φ_1 direction increases until it blocks the motion of the particle. From this point on ($\Phi_{ext} \lesssim \Phi_0/2$), the bias current has to be increased again until the particle can leave the side well B by TA and start running down the potential.

Once the external flux is turned negative from zero ($\Phi_{ext} < 0$), the direction of the circulating current is reversed and so is the change of barrier height in the φ_1 and φ_2 direction. Hence, the switching current due to MQT increases until it reaches its maximum and classical TA becomes dominant. From here, the switching current of the dc SQUID decreases again and follows the well-known flux dependence (cf. Ref. [14]). The barrier in the classical direction decreases up to the flux $\Phi_{ext} \approx -\Phi_0/2$ and so does the switching current of the SQUID. In the following, we corroborate this picture by demonstrating the consistency of the data with predicted TA and MQT decay rates, respectively.

The mean switching current shown in Fig. 3 is extracted from switching current histograms which in turn are related to escape rates [5]. An expression for the thermal escape rate that takes into account the nontrivial, 2D potential has been put forward in Ref. [14],

$$\Gamma_{TA} = \frac{\omega_p}{2\pi}\frac{\omega_{w\perp}}{\omega_{s\perp}}\exp\left(-\frac{\Delta U}{k_B T}\right), \tag{4}$$

where the current dependent potential height ΔU and plasma frequency ω_p additionally depend on the direction θ of the decay [14]. The angle θ is measured with respect to the φ_1 axis. It changes with applied flux Φ_{ext} and is also affected by a possible asymmetry in the critical currents. Additionally, we have to introduce the effective capacitance $C_{eff} = C_1 \cos^2\theta + C_2 \sin^2\theta$ along the direction of escape into the expression for ω_p. This value is calculated from the kinetic energy of the effective 1D problem in direction θ. For our weakly coupled SQUID, the ratio of transverse frequencies $\omega_{w\perp}/\omega_{s\perp}$ in the well and around the saddle can be set to unity.

Equation (4) is used to fit the measured escape rates corresponding to the data points in the black oval in Fig. 3. It yields a mean critical current $I_0 = 482 \pm 6$ nA and a current asymmetry parameter $\alpha = 0.053 \pm 0.0004$, such that $I_{c1} = (1-\alpha)I_0 = 456$ nA and $I_{c2} = (1+\alpha)I_0 = 508$ nA. This result is in agreement with the designed value of $I_{c,nom} = 560$ nA within the unavoidable uncertainties in the fabrication process.

The effective junction temperature T is used as an additional fit parameter. The mean value of the four values

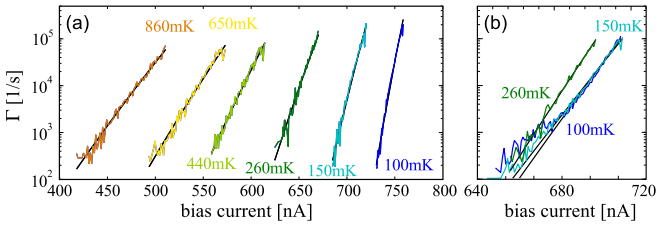

FIG. 4 (color online). (a) TA rates at $\Phi_{\rm ext}/\Phi_0 = -0.24$. (b) MQT rates at $\Phi_{\rm ext}/\Phi_0 = 0.24$ for the three lowest temperatures. Measured TA and MQT rates are in color, fit results for the respective temperatures in black.

of T resulting from measurements at different flux values $\Phi_{\rm ext}$ is determined and the standard deviation found to be less than 4%. The resulting mean temperatures (as given in Figs. 3 and 4) reflect the electron temperatures of the junctions and are, as expected, higher than the measured cryostat temperature. In Fig. 4(a), the measured escape rates (in color) and the fit results (black) are presented for a flux value of $\Phi_{\rm ext}/\Phi_0 = -0.24$.

The decay via quantum tunneling has to account for the two-dimensionality of the situation as well. Following Refs. [19,20], the quantum escape rate

$$\Gamma_{\rm MQT} = \frac{\omega_p}{2\pi}\exp\left[-\frac{36\Delta U}{5\hbar\omega_p}\left(1+\frac{0.87\omega_p}{\omega_c}\right)\right] \qquad (5)$$

involves again the θ-dependent potential height ΔU and plasma frequency ω_p from Ref. [14], only here, the angle θ has to be set to $\pi/2$, since tunneling is only possible for $\varphi = \text{const}$ [15]. The second term in the exponent of Eq. (5) takes into account the non-negligible effect of dissipation [2,21] (for the classical junction the ratio ω_p/ω_c is small, allowing us to neglect damping [22]). Since instanton splitting [23,24] is not possible in the case of a capacitively asymmetric dc SQUID [15], the additional prefactor $f_{\rm 2D}$ used in Refs. [19,20] is set to unity and omitted in Eq. (5).

Equation (5) is used to fit the measured escape rates at different flux values (black rectangle in Fig. 3) on the negative slope. The result of this fit and the corresponding measured escape rates at $\Phi_{\rm ext}/\Phi_0 = 0.24$ are shown in Fig. 4(b) for the three lowest temperatures. The deviation of the 270 mK line is most probably due to the onset of thermally assisted tunneling. The resulting values of the fit parameters, i.e., mean critical current I_0 and asymmetry parameter α for the two lowest temperatures agree within 4% with the results obtained from the TA fit. The fitted value for the resistance $R = 195 \pm 16\,\Omega$ is below the zero frequency value given in Table I. We attribute this discrepancy to the small capacitance of JJ_2 which results in a very high plasma frequency (cf. Table I). At such high frequencies, the biasing circuitry provides the dominating admittance, which leads, in our setup, to an effective resistance of $R \approx 200\,\Omega$. In fact, we have observed the related effect of classical phase diffusion [25] for a similar dc SQUID ($L = 8$ nH) with nominally the same junction areas and capacitances, fabricated on the same wafer. A large damping is also consistent with a reduced crossover temperature compared to $T_{\rm cr,nom}(j_{\rm sw}) \approx 660$ mK. It lies between 260 mK $< T_{\rm cr} <$ 440 mK according to Fig. 3.

Figure 5 further underlines the difference in escape statistics of TA and MQT. It shows the full switching histogram instead of only the mean switching current at the lowest temperature over several periods of Φ_0. The height of the histogram in every current bin with a finite number of events is presented in gray scale. Darker gray corresponds to a larger number of switching events in the respective bin. A broadening and splitting into two peaks is observed in a small range around odd integer multiples of $\Phi_0/2$ since the system has a non-negligible probability of being retrapped in a side minimum instead of the main one. The different widths of the histograms on positive and negative slopes correspond to the two different escape processes in the asymmetric dc SQUID. Measurements for positive and negative current polarity confirm that the observed MQT and TA behavior are indeed related to the escape direction. Dashed black lines show again the calculated flux dependence of the fluctuation free critical current for a dc SQUID. The switching current on the MQT slope is considerably suppressed compared to the calculated critical current. Thus, Fig. 5 clearly shows that the virtual particle escapes out of a minimum which, classically, it could not leave, yet.

In conclusion, we investigated the switching characteristics of a dc SQUID with a strong capacitive asymmetry. Flux-dependent measurements show a clear difference of the switching current distribution on positive and negative slopes. Temperature dependent measurements and the comparison with theory attribute the switching on positive slopes to TA and on negative slopes to MQT. Thus, depending on the magnetic field, our device shows either MQT or TA, both at the same temperature. Returning to the

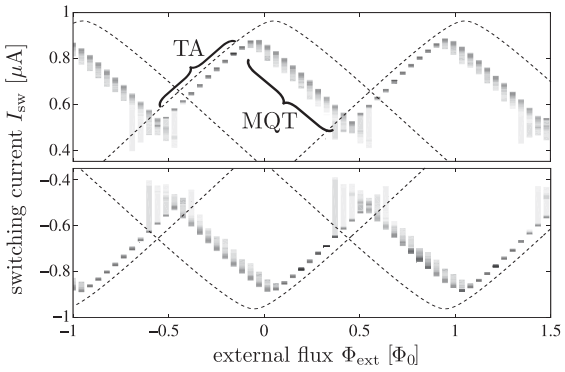

FIG. 5. Dependence of the switching current $I_{\rm sw}$ on flux $\Phi_{\rm ext}$ for positive and negative current polarity. The bars represent the recorded switching current histograms. The intensity of gray illustrates the number of counts per current bin. Dashed lines display the theoretically expected behavior in the absence of fluctuations for the extracted critical currents.

virtual particle picture, we showed that a particle with strongly anisotropic mass displays either quantum mechanical or classical behavior, depending on the direction of escape. Hence, coupling a classical to a quantum mechanical degree of freedom can facilitate the escape of a particle in a 2D potential considerably compared to a purely classical system. We thus experimentally verified the predictions made by Thomann *et al.* [1] and, on a less serious note, conclude that Baron Münchhausen could have pulled himself and his horse out of the swamp.

The authors acknowledge interesting discussions with B. I. Ivlev. Susanne Butz acknowledges the financial support by the Landesgraduiertenförderung Baden-Württemberg. This work was partially supported by the Ministry of Education and Science of the Russian Federation under Contract No. 11.G34.31.0062.

*alexey.ustinov@kit.edu
†Present address: École Polytechnique Fédérale de Lausanne (EPFL), CH-1015 Lausanne, Switzerland.
‡Present address: Walther-Meissner-Institut, Bayerische Akademie der Wissenschaften, 85748 Garching, Germany.

[1] A. U. Thomann, V. B. Geshkenbein, and G. Blatter, Phys. Rev. B **79**, 184515 (2009).
[2] A. O. Caldeira and A. Leggett, Ann. Phys. (N.Y.) **149**, 374 (1983).
[3] A. I. Larkin and Yu. N. Ovchinnikov, Zh. Eksp. Teor. Fiz. **85**, 1510 (1983) [Sov. Phys. JETP **58**, 876 (1983)].
[4] B. D. Josephson, Adv. Phys. **14**, 419 (1965).
[5] T. A. Fulton and L. N. Dunkleberg, Phys. Rev. B **9**, 4760 (1974).
[6] R. F. Voss and R. A. Webb, Phys. Rev. Lett. **47**, 265 (1981).
[7] M. H. Devoret, J. M. Martinis, and J. Clarke, Phys. Rev. Lett. **55**, 1908 (1985).
[8] M. Rudolph, J. Nagel, J. M. Meckbach, M. Kemmler, M. Siegel, K. Ilin, D. Koelle, and R. Kleiner, Appl. Phys. Lett. **101**, 052602 (2012).
[9] D. F. Sullivan, S. K. Dutta, M. Dreyer, M. A. Gubrud, A. Roychowdhury, J. R. Anderson, C. J. Lobb, and F. C. Wellstood, J. Appl. Phys. **113**, 183905 (2013).
[10] D. Vion, A. Aassime, A. Cottet, P. Joyez, H. Pothier, C. Urbina, D. Esteve, and M. H. Devoret, Science **296**, 886 (2002).
[11] M. L. Della Rocca, M. Chauvin, B. Huard, H. Pothier, D. Esteve, and C. Urbina, Phys. Rev. Lett. **99**, 127005 (2007).
[12] R. W. Simmonds, K. M. Lang, D. A. Hite, S. Nam, D. P. Pappas, and J. M. Martinis, Phys. Rev. Lett. **93**, 077003 (2004).
[13] T. A. Palomaki, S. K. Dutta, H. Paik, H. Xu, J. Matthews, R. M. Lewis, R. C. Ramos, K. Mitra, P. R. Johnson, F. W. Strauch, A. J. Dragt, C. J. Lobb, J. R. Anderson, and F. C. Wellstood, Phys. Rev. B **73**, 014520 (2006).
[14] V. Lefevre-Seguin, E. Turlot, C. Urbina, D. Esteve, and M. H. Devoret, Phys. Rev. B **46**, 5507 (1992).
[15] B. Ivlev and J. P. Palomares-Baez, Phys. Rev. B **82**, 184513 (2010).
[16] R. Dolata, H. Scherer, A. B. Zorin, and J. Niemeyer, J. Appl. Phys. **97**, 054501 (2005).
[17] M. Tinkham, *Introduction to Superconductivity* (Dover, Mineola, NY, 2004), p. 261.
[18] A. Wallraff, A. Lukashenko, C. Coqui, A. Kemp, T. Duty, and A. V. Ustinov, Rev. Sci. Instrum. **74**, 3740 (2003).
[19] S. X. Li, Y. Yu, Y. Zhang, W. Qiu, S. Han, and Z. Wang, Phys. Rev. Lett. **89**, 098301 (2002).
[20] F. Balestro, J. Claudon, J. P. Pekola, and O. Buisson, Phys. Rev. Lett. **91**, 158301 (2003).
[21] J. M. Martinis, M. H. Devoret, and J. Clarke, Phys. Rev. B **35**, 4682 (1987).
[22] Y. Yoon, S. Gasparinetti, M. Möttönen, and J. P. Pekola, J. Low Temp. Phys. **163**, 164 (2011).
[23] A. Schmid, Ann. Phys. (N.Y.) **170**, 333 (1986).
[24] B. I. Ivlev and Y. N. Ovchinnikov, Zh. Eksp. Teor. Fiz. **93**, 668 (1987) [Sov. Phys. JETP **66**, 378 (1987)].
[25] R. L. Kautz and J. M. Martinis, Phys. Rev. B **42**, 9903 (1990).